ISSN1027-5495. Functional Materials, 31, No.1 (2024), p. 96-109
doi:http://dx.doi.org/10.15407/fm31.01.96

Three-dimensional magnetohydrodynamic Casson flow of a dust nanofluid over a stretching porous sheet: exact solutions

M.I. Kopp[1], V.V. Yanovsky[1,2]

[1]Institute for Single Crystals, NAS Ukraine, Nauky Ave. 60, Kharkov 61001, Ukraine
[2]V.N. Karazin Kharkiv National University 4 Svobody Sq., Kharkov 61022, Ukraine

Received October 8, 2023

In this paper, the stationary three-dimensional (3D) magnetohydrodynamic Casson flow of a nanofluid containing dust particles over a porous, linearly stretching sheet is considered. The sheet is assumed to be stretched in both directions along the *xy* plane. The nanofluid is presented as a suspension of water-based nanoparticles. In this study, we investigate the effects of nanoparticle size and inter-particle distance factors on the properties of the nanofluid flow. The mathematical model contains the basic equations in the form of three-dimensional partial differential equations for the fluid and dust phases, and these equations are transformed into dimensionless ordinary-dimensional equations using an appropriate similarity transformation. Exact analytical solutions to this boundary value problem are obtained. The effects of various physical values on dust and nanofluid velocities are discussed in detail, including the magnetic parameter, Casson parameter, porosity parameter, fluid-particle interaction parameter, mass concentration of dust particles, and nanoparticle size. The current analytical solutions show good agreement with previously published numerical investigations in a few particular cases.

Keywords: MHD Casson flow, nanofluid, dust particles, nanoparticle size, stretching sheet, analytical solutions.

Тривимірне магнітогідродинамічне течія Кессона пильової нанорідини над пористим листом, що розтягується: точні рішення. *М. Й. Копп, В. В. Яновський*.

У цій роботі розглядається стаціонарна тривимірна (3D) магнітогідродинамічна течія Кассона нанорідини, що містить пилові частинки, над пористим листом, що лінійно розтягується. Передбачається, що лист розтягнутий в обох напрямках вздовж площини *xy*. Основні рівняння двофазної моделі є рівняннями в часткових похідних, які перетворюються на звичайні рівняння з використанням перетворень подібності. Нанорідина представлена як суспензія наночастинок на водній основі. У цій роботі ми досліджуємо вплив розміру наночастинок та факторів відстані між частинками на властивості потоку нанорідини. Отримано точні аналітичні рішення цієї крайової задачі. Детально обговорюється вплив різних фізичних величин на швидкість пилу та нанорідкості, включаючи магнітний параметр, параметр Кессона, параметр пористості, параметр взаємодії рідина-частинка, масову концентрацію пилових частинок та розмір наночастинок. Отримані аналітичні рішення показують гарну згоду з чисельними результатами раніше опублікованих робіт.

1. Introduction

The problem of the boundary flow of non-Newtonian dusty fluids has attracted more and more attention during the past decades. A two-phase medium made up of a continuous fluid and a discrete (solid) phase of particles is called a "dusty fluid whether it is Newtonian or non-Newtonian. Dusty fluid flows have been observed in processes such as oil transportation, wastewater treatment, nuclear reactor cooling, powder technology, paint spraying, solid propellant nozzles, and guided missile ejections. Since crude oil is produced in the pores of reservoir rocks, the flow of fluid through the porous medium has become an important issue. The above phenomena stimulated researchers to consider the issues of modeling, solving, and analysing the flow of dusty fluids. As a result, new combined fluid models with different rheological characteristics have appeared, such as, for example, the dusty Casson nanofluid, which make it possible to effectively describe complex technological processes.

Saffman [1] was the first to study the laminar flow of a dusty Newtonian fluid. Chakrabarti [2] investigated the flow of dusty gas at the boundary layer. Datta and Mishra [3] discussed the flow of a dusty liquid across a semi-infinite plate. Numerous technical applications, including those for reactor cooling, power generators, magnetohydrodynamic (MHD) pumps, the oil industry, and heat exchanger design, make the study of MHD flow crucial. MHD flows also have a significant impact on metrology, the motion of the earth's core, astronomy, solar physics, and geophysics. Many researchers started looking into the hydromagnetic fluxes of a dusty fluid because of the importance of the MHD flow.

One of the earliest studies on boundary layer flow on solid surfaces was done by Sakiadis [4] and Tsou et al. [5]. For a two-dimensional stationary flow in a boundary layer produced by an expanding surface, Crane [6] obtained an analytical solution. These publications [4]-[6] inspired many researchers to study various aspects of this problem, taking into account heat and mass transfer, MHD effects, chemical processes, suction/injection, mass transpiration, non-Newtonian fluids, and other situations. Due to the wide range of applications, studies on the two-dimensional boundary layer flow generated by stretching surfaces are extensively conducted with different fluids under varying situations. This topic has been the subject of a significant number of papers for a very long time. As a result, the studies that discuss three-dimensional MHD flows of a non-Newtonian (Casson) fluid over a stretched surface will be the main focus of the review section of this study. In the Casson viscous fluid flow model, the shear stresses are greater than the yield strength. If the shear stresses are less than the yield strength, then the Casson fluid behaves like a solid. Casson's fluid is commonly found in the food industry, where products such as jellies, tomato sauce, honey, and concentrated fruit juices are produced. In medicine, human blood has the properties of Casson's fluid. The flow of a viscous fluid over a surface that is either stretched or compressed is important for a variety of processes, such as the production of glass, fiber, plastic, and rubber materials and the melting of high-molecular-weight polymers. Wang [7] obtained an exact similarity solution of the Navier-Stokes equations for a three-dimensional flow of a boundary layer of a viscous fluid over a flat surface that is stretched with a linear velocity in two lateral directions. The concepts presented in this paper provided inspiration for the study of three-dimensional flows under more complex physical circumstances. The problem of steady laminar three-dimensional MHD boundary layer flow and heat transfer over a stretching surface in a viscoelastic fluid was investigated by Ahmad and Nazar [8]. They obtained coupled non-linear ordinary differential equations to describe the flow, which they solved numerically using the finite difference scheme known as the Kellerbox method.

A colloidal suspension of a nanoscale particle in a basic fluid is known as a "nanofluid"[9]. Metals, oxides, carbides, and carbon nanotubes are among the most commonly used nanoparticles, with water and ethylene glycol serving as the base fluids. For the effective transmission of thermal energy, nanofluids have a higher thermal conductivity than ordinary fluids. A suspension of nanosized particles can affect the viscous and rheological properties of a nanofluid since an increase in the volume fraction of nanoparticles increases the dynamic viscosity.

Ramzan et al. [10] investigated the three-dimensional flow of a viscoelastic fluid, taking into account the Soret and Dufour effects. In [10], solution expressions of velocity, temperature and nanoparticle concentration are computed via homotopy analysis method (HAM). Ashraf et al. [11] considered the heat and mass transfer effects in the three-dimensional flow of a Maxwell fluid over a stretching surface with

convective boundary conditions. Nadeem et al. [12] investigated the Casson fluid flow on a permeable sheet caused by sheet stretching in the x and y directions in a transverse magnetic field. In a later study, Nadeem et al. [13] extended the study to a Casson nanofluid over a linearly stretching sheet, taking into account surface convective conditions. Mahanta and Shaw [14] investigated a three-dimensional Casson fluid flow past a porous linearly stretching sheet, introducing a convective boundary condition at the surface where the fluid's thermal conductivity varies linearly concerning temperature. They used the Spectral Relaxation Method (SRM) to solve the governing equations, and computations were performed for the velocity and temperature fields for different parameters. Krishna [15] solved MHD Casson fluid flow past a porous, linearly stretching surface with wall mass transfer analytically. In [15] the fluid velocity and skin friction coefficient were calculated, and it was demonstrated that increasing the Casson and porosity parameters suppressed the velocity field. Madhusudan et al. [16] numerically studied the convective, three-dimensional, electrically conducting Casson nanofluid flow over an exponentially stretching sheet embedded in a saturated porous medium and subjected to thermal as well as solute slip in the presence of an externally applied transverse magnetic field. Ibrahim and Anbessa [17] investigated the three-dimensional MHD mixed convection flow of Casson nanofluid over an exponentially stretching sheet using the impacts of Hall and ion slip currents, taking into account thermal radiation and the heat source.

According to the reviewed literatures above, numerical solutions provide the foundation for most investigations. The advantage of an exact analytical solution is that it can explain the physics of fluid flow. The correct response may also be used as a starting point for additional numerical and approximative investigations.

Jalil et al. [18] gave an exact analytical solution for the MHD boundary flow of a dusty liquid over an extension surface. The mathematical methodology used in [18] consists of transforming the basic equations into a self-similar form using known similarity transformations. The coupled equations are then analytically solved using Crane's [6] solution as a guide. Vishalakshi et al. [19] obtained exact analytical solutions for the three-dimensional flow of a non-Newtonian fluid due to a porous stretching/shrinking sheet. The importance of paper [19] is to examine the problem analytically and find the domain in terms of mass transpiration that is used in the heat transfer equation to analyze the heat equation. Mahabaleshwar et al. [20] conducted an investigation of the exact analytical solution for velocity and concentration field for 3D MHD flow viscoelastic hybrid nanofluid due to a porous sheet that stretched/shrunk along both x and y axes with linear velocity and Navier slip. Exact analytical solutions in exponential and hypergeometric form for velocity and concentration fields were obtained in [20]. The flow of Marangoni convection MHD Casson fluid with carbon nanotubes under the effects of transpiration and radiation was analyzed by Vishalakshi et al. [21]. The ordinary differential equations (ODEs) obtained in [21] are solved analytically, first using the momentum equation to obtain the solution domain, and then using this domain, the energy equation is solved to obtain the temperature profile in terms of the Laguerre polynomial. Recently, Khan et al. [22] found an exact solution of a Casson fluid flow induced by dust particles with hybrid nanofluid over a stretching sheet under a Lorentz force. They obtained the analytical solutions of momentum equations for the fluid and dust phases velocities of the normal nanofluid (Fe_3O_4/H_2O) and hybrid nanofluid (Fe_3O_4-MWCNT/H_2O). Kopp et al. [23] was obtained the analytical solution of the three-dimensional MHD flow of the Casson ternary hybrid nanofluid over a linearly deformable surface with the effect of mass transpiration. The authors [23] considered several variants of linear stretching/shrinking sheets in the lateral directions x and y. They found that for the cases of stretching/streching, stretching/shrinking, and shrinking/stretching sheets, the absolute values of the skin friction coefficients $-f''(0)$ and $-g''(0)$ decreased with an increase in the volume fraction of less dense nanoparticles. However, in the case of a shrinking/shrinking sheet, the absolute values of skin friction coefficients $-f''(0)$ and $-g''(0)$ increased with an increase in the volume fraction of less dense nanoparticles.

The above review of the literature showed that most studies are based on finding numerical as well as approximate solutions. The search for exact analytical solutions is associated with difficulties due to the nonlinearity of the coupled differential equations. Unlike the previous analytical works [18],[22],[23] this work is devoted to an analytical study of the three-dimensional MHD Casson flow of a dusty nanofluid due to stretching of a porous surface. In this study, we will apply a methodology based on Crane's exact

analytical solutions. In addition, the novelty of this study is to explain how the size of nanoparticles affects the properties of a dusty nanofluid flow. Using various physical parameters, an exact check of the problem is performed, and velocity profiles and skin friction coefficients in the x and y directions are studied.

2. Mathematical formulation of the problem

Consider a stationary, three-dimensional, incompressible, laminar flow of a Casson nanofluid containing dust particles in two lateral directions over a linearly stretching sheet. The nanofluid includes solid copper nanoparticles and water as the base fluid. It is assumed that dust particles have a spherical shape, uniform size, and constant density. Fig. 1 shows the conceptual flow configuration of the nanofluid and dust particles of the problem under consideration. A constant magnetic field B_0 is applied in the direction normal to the fluid flow. The magnetic Reynolds number is assumed to be small, so the induced magnetic field is neglected. Let $U_w = ax$ and $V_w = by$ represent the fluid velocity along the stretching sheet in the x and y directions, where a and b are constants. An isotropic, incompressible Casson fluid's rheological equation has the following structure (see, for example, [14]):

$$\tau_{ij} = \begin{cases} 2\left(\mu + \frac{P_y}{\sqrt{2\pi}}\right) e_{ij}, \pi > \pi_c \\ 2\left(\mu + \frac{P_y}{\sqrt{2\pi_c}}\right) e_{ij}, \pi < \pi_c \end{cases} \tag{1}$$

$$e_{ij} = \frac{1}{2}\left(\frac{\partial v_i}{\partial x_j} + \frac{\partial v_j}{\partial x_i}\right),$$

where τ_{ij} is the $(i,j)^{\text{th}}$ component of the stress tensor, μ is the dynamic viscosity of a viscoplastic fluid, P_y is the yield stress of the fluid, $\pi = e_{ij}e_{ij}$ is the product of the component of deformation rate with itself, e_{ij} is the $(i,j)^{\text{th}}$ component of deformation rate, and π_c is the critical value of π depends on non-Newtonian model.

The governing equations for the flow and dusty fluid under the aforementioned assumptions are as follows:

For the fluid phase:

$$\frac{\partial u}{\partial x} + \frac{\partial v}{\partial y} + \frac{\partial w}{\partial z} = 0 \tag{2}$$

$$u\frac{\partial u}{\partial x} + v\frac{\partial u}{\partial y} + w\frac{\partial u}{\partial z} = \frac{\mu_{nf}}{\rho_{nf}}\left(1 + \frac{1}{\Lambda}\right)\frac{\partial^2 u}{\partial z^2} - \frac{\mu_{nf}}{\widetilde{k}\rho_{nf}}u - \\ - \frac{\sigma_{nf}}{\rho_{nf}}B_0^2 u + \frac{KN}{\rho_{nf}}(u_p - u) \tag{3}$$

$$u\frac{\partial v}{\partial x} + v\frac{\partial v}{\partial y} + w\frac{\partial v}{\partial z} = \frac{\mu_{nf}}{\rho_{nf}}\left(1 + \frac{1}{\Lambda}\right)\frac{\partial^2 v}{\partial z^2} - \frac{\mu_{nf}}{\widetilde{k}\rho_{nf}}v - \\ - \frac{\sigma_{nf}}{\rho_{nf}}B_0^2 v + \frac{KN}{\rho_{nf}}(v_p - v) \tag{4}$$

For the dust phase:

$$\frac{\partial u_p}{\partial x} + \frac{\partial v_p}{\partial y} + \frac{\partial w_p}{\partial z} = 0 \tag{5}$$

$$u_p\frac{\partial u_p}{\partial x} + v_p\frac{\partial u_p}{\partial y} + w_p\frac{\partial u_p}{\partial z} = \frac{KN}{\rho_p}(u - u_p) \tag{6}$$

$$u_p\frac{\partial v_p}{\partial x} + v_p\frac{\partial v_p}{\partial y} + w_p\frac{\partial v_p}{\partial z} = \frac{KN}{\rho_p}(v - v_p) \tag{7}$$

where (u, v, w) and (u_p, v_p, w_p) are the velocities of nanofluid and dust particles along the x, y, and z-directions. Next, $\rho_{nf}, \mu_{nf}, \sigma_{nf}$ are the density, dynamic viscosity, and electrical conductivity of nanofluid,

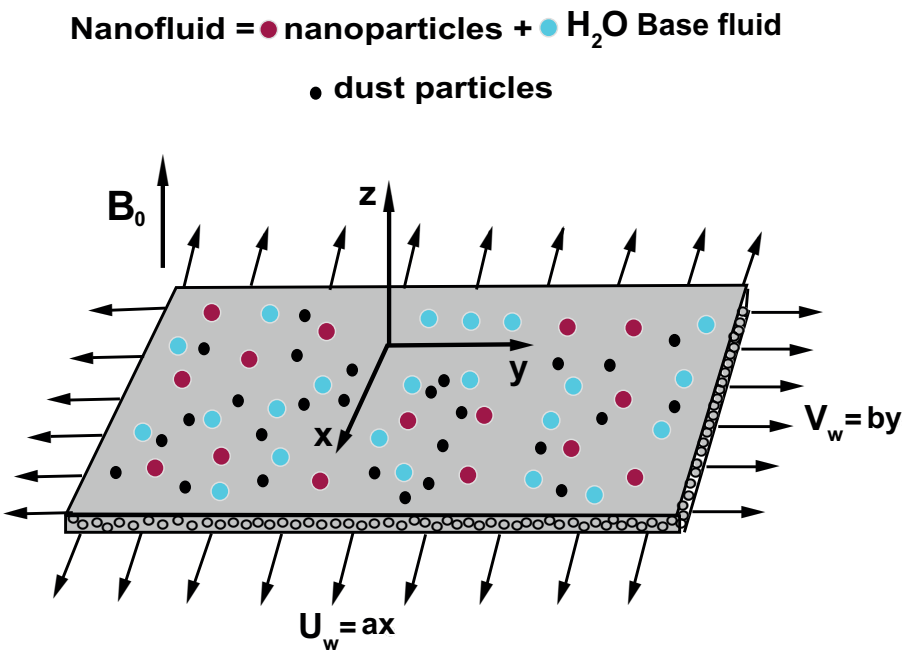

Fig.1. Schematic diagram for the three-dimensional flow problem.

respectively. Λ is the Casson (non-Newtonian) fluid parameter, $\widetilde{k}$ is the permeability of a porous medium, B_0 is the magnetic induction. $K = 6\pi\mu_f r$ is Stokes drag constant, r – radius of dust particles, N and ρ_p are the dust particle number and the density of the dust particle, respectively.

We take into consideration the following slip boundary conditions for the flow under investigation:

$$u = U_w, \quad v = V_w, \quad w = 0 \quad \text{at} \quad z = 0 \tag{8}$$

$$u = u_p \to 0, \; v = v_p \to 0, \quad w = w_p \quad \text{at} \quad z \to \infty \tag{9}$$

The relationship between the dynamic viscosities, densities, and electrical conductivities of the nanofluid and the base fluid are determined according to the works [24]

1. Dynamic viscosity

$$\epsilon_1 = \frac{\mu_{nf}}{\mu_f} = 1 + 2.5\phi_s + 4.5\left[\frac{h}{d_n}\left(2 + \frac{h}{d_n}\right)\left(1 + \frac{h}{d_n}\right)^2\right]^{-1} \tag{10}$$

2. Density

$$\epsilon_2 = \frac{\rho_{nf}}{\rho_f} = 1 - \phi_s + \phi_s\frac{\rho_s}{\rho_f} \tag{11}$$

3. Electrical conductivity

$$\epsilon_3 = \frac{\sigma_{nf}}{\sigma_f} = 1 + \frac{3\phi_s\left(\frac{\sigma_s}{\sigma_f} - 1\right)}{\left(\frac{\sigma_s}{\sigma_f} + 2\right) - \phi_s\left(\frac{\sigma_s}{\sigma_f} - 1\right)} \tag{12}$$

where ϕ_s is the nanoparticle concentration, d_n depicts the nanoparticle's diametr, and h is the interparticle distance. Next, ρ_f is the base fluid density, ρ_s is density of nanoparticle, σ_f depicts the electric conductance of the base fluid, and σ_s is the electric conductance of nanoparticle. Table 2 shows the physical characteristics of some types of nanofluids. To make the analysis simpler, the similarity transformation

Table 1. Physical properties of the nanoparticles and the base fluid.

Property	H_2O	Al_2O_3
$\rho[kg \cdot m^{-3}]$	997.1	3970
$\sigma[S \cdot m^{-1}]$	$5.5 \cdot 10^{-6}$	$5.96 \cdot 10^{7}$

listed below is used

$$u = axf'(\eta),\ u_p = axF'(\eta),\ v = ayg'(\eta),\ v_p = ayG'(\eta),$$
$$w = -\sqrt{a\nu_f}(f(\eta)+g(\eta)),\ w_p = -\sqrt{a\nu_f}(F(\eta)+G(\eta)),\ \eta = z\sqrt{\frac{a}{\nu_f}}, \tag{13}$$

where f, g, F, G are the dimensionless functions, η is the similarity variable, ν_f is the kinematic viscosity of the base fluid. Primes denote differentiation with regard to η in this context. Equations (3)-(4) and (6)-(7) are converted into dimensionless ODEs using Eqs. (10)-(13), and the continuity equations (2) and (5) is automatically satisfied by using Eq. (13). Then, equations for the fluid and dust phases (3)-(4) and (6)-(7) are reduced to the following equations:

$$\left(1+\frac{1}{\Lambda}\right)\frac{\epsilon_1}{\epsilon_2}f''' + (f+g)f'' - f'^2 - \left(\frac{\epsilon_3}{\epsilon_2}M + \frac{\epsilon_1}{\epsilon_2}\widetilde{K}\right)f' + \frac{\beta_v l}{\epsilon_2}(F'-f') = 0 \tag{14}$$

$$\left(1+\frac{1}{\Lambda}\right)\frac{\epsilon_1}{\epsilon_2}g''' + (f+g)g'' - g'^2 - \left(\frac{\epsilon_3}{\epsilon_2}M + \frac{\epsilon_1}{\epsilon_2}\widetilde{K}\right)g' + \frac{\beta_v l}{\epsilon_2}(G'-g') = 0 \tag{15}$$

$$F'^2 - (F+G)F'' - \beta_v(f'-F') = 0 \tag{16}$$

$$G'^2 - (F+G)G'' - \beta_v(g'-G') = 0 \tag{17}$$

where

$$M = \frac{B_0^2\sigma_f}{a\rho_f},\quad \widetilde{K} = \frac{\nu_f}{a\widetilde{k}},\quad \beta_v = \frac{KN}{a\rho_p},\quad l = \frac{\rho_p}{\rho_f}.$$

The magnetic parameter, porosity parameter, momentum dust parameter, and mass concentration of dust particles, respectively, are designated by the dimensionless parameters $M, \widetilde{K}, \beta_v$, and l. By applying Eq. (13) to Eqs. (8)-(9), dimensionless boundary constraints are obtained.

$$f(0) = 0,\quad f'(0) = 1,\quad g(0) = 0,\quad g'(0) = c \quad \text{at} \quad \eta = 0 \tag{18}$$

$$f'(\eta) \to 0,\ g(\eta) \to 0,\ f(\eta) \to F(\eta),\ g(\eta) \to G(\eta) \quad \text{at} \quad \eta \to \infty \tag{19}$$

where $c = b/a$ is stretching ratio parameter.

To solve a number of engineering problems, it is necessary to estimate the value of the skin friction coefficient. Skin friction is important in calculating surface drag. The local skin friction coefficients in the x and y directions are given by [14]:

$$C_{fx} = \frac{\tau_{wx}}{\rho_f U_w^2},\quad C_{fy} = \frac{\tau_{wy}}{\rho_f U_w^2}, \tag{20}$$

where τ_w is the wall shear stress. The wall shear stresses along the x and y directions are denoted by

$$\tau_{wx} = \mu_{nf}\left(1+\frac{1}{\Lambda}\right)\left(\frac{\partial u}{\partial z}\right)_{z=0},\quad \tau_{wy} = \mu_{nf}\left(1+\frac{1}{\Lambda}\right)\left(\frac{\partial v}{\partial z}\right)_{z=0}.$$

Thus, the skin friction coefficients C_f along the x and y axes are expressed as follows:

$$C_{fx}\sqrt{Re_x} = \frac{\mu_{nf}}{\mu_f}\left(1+\frac{1}{\Lambda}\right)f''(0),\quad C_{fy}\sqrt{Re_x} = \frac{\mu_{nf}}{\mu_f}\left(1+\frac{1}{\Lambda}\right)\left(\frac{y}{x}\right)g''(0), \tag{21}$$

where $Re_x = U_w x/\nu_f$ is the local Reynolds number.

3. Method of solution

This section explains a method for locating precise nonlinear solutions for the fluid and dust phases (14)-(17) that are related to the boundary conditions (18)-(19). Based on Crane's [6] solution, we suggest that the general solution of equations (14)-(17) can be found in the exponential form:

$$f(\eta) = A_1 + A_2 e^{-\beta\eta}, \quad g(\eta) = A_3 + A_4 e^{-\beta\eta},$$
$$F(\eta) = A_5 + A_6 e^{-\beta\eta}, \quad G(\eta) = A_7 + cA_8 e^{-\beta\eta}, \tag{22}$$

where $A_1, A_2, A_3, A_4, A_5, A_6, A_7, A_8$ are the arbitrary constants. Applying boundary conditions (18)-(19) to solutions (22), we obtain expressions for the coefficients:

$$A_1 = \frac{1}{\beta}, \quad A_2 = -\frac{1}{\beta}, \quad A_3 = \frac{c}{\beta},$$
$$A_4 = -\frac{c}{\beta}, \quad A_5 = A_1 = \frac{1}{\beta}, \quad A_7 = A_3 = \frac{c}{\beta}. \tag{23}$$

The coefficients A_6 and A_8 are then determined by inserting solutions (22) and (23) into equations (14)-(15). As a result, we obtain the following equation for A_6 and A_8:

$$(1-c)\left(\alpha_1\beta^2 - 1 - c - \alpha_2 - \alpha_3\right) - \alpha_3\beta(A_6 - cA_8) = 0, \tag{24}$$

where

$$\alpha_1 = \left(1 + \frac{1}{\Lambda}\right)\frac{\epsilon_1}{\epsilon_2}, \quad \alpha_2 = \frac{\epsilon_3}{\epsilon_2}M + \frac{\epsilon_1}{\epsilon_2}\widetilde{K}, \quad \alpha_3 = \frac{\beta_v l}{\epsilon_2}.$$

Substituting solutions (22)-(23) into equations (16)-(17), we get

$$A_6 - cA_8 = -\frac{\beta_v(1-c)}{\beta(1+c+\beta_v)}, \tag{25}$$

here

$$A_6 = -\frac{\beta_v}{\beta(1+\beta_v)}, \quad cA_8 = -\frac{c\beta_v(2+\beta_v)}{\beta(1+\beta_v)(1+c+\beta_v)}.$$

From expressions (24) and (25), one can easily find the value β:

$$\beta = \pm\sqrt{\frac{1}{\alpha_1}\left(1 + c + \alpha_2 + \alpha_3 - \frac{\alpha_3\beta_v}{1+c+\beta_v}\right)} \tag{26}$$

Obviously, only positive real values of $\beta > 0$ are required. In the case of a two-dimensional steady flow $c \to 0$ expressions (25) and (26) coincide with the paper's [22] results.

Finally, we obtain the final form of exact analytical solutions for the fluid and dust phases by substituting the values of the coefficients from (25) and (26) into expressions (22):

$$f(\eta) = \frac{1}{\beta}(1 - e^{-\beta\eta}), \quad g(\eta) = \frac{c}{\beta}\left(1 - e^{-\beta\eta}\right),$$
$$F(\eta) = \frac{1}{\beta}\left(1 - \frac{\beta_v e^{-\beta\eta}}{1+\beta_v}\right),$$
$$G(\eta) = \frac{c}{\beta}\left(1 - \frac{\beta_v(2+\beta_v)e^{-\beta\eta}}{(1+\beta_v)(1+c+\beta_v)}\right). \tag{27}$$

By differentiating expressions (27) with respect to η, we can determine the velocity profiles in the x and y directions for the fluid and dust phases:

$$f'(\eta) = e^{-\beta\eta}, \; g'(\eta) = ce^{-\beta\eta}, \; F'(\eta) = \frac{\beta_v e^{-\beta\eta}}{1+\beta_v},$$

$$G'(\eta) = \frac{c\beta_v(2+\beta_v)e^{-\beta\eta}}{(1+\beta_v)(1+c+\beta_v)}. \tag{28}$$

Differentiating expressions (28) by variable η yields the expressions $-f''(0)$ and $-g''(0)$, which are considered necessary for calculating fluid phase skin friction coefficients in both lateral directions:

$$-f''(0) = \beta, \quad -g''(0) = c\beta. \tag{29}$$

4. Results and discussion

In this section, we discuss the results obtained from the analytical solution (26)-(29) for the steady flow of a nanofluid and (Al_2O_3-H_2O) dust particles in both lateral directions. The effects of the non-Newtonian (Cassonian) parameter Λ, the magnetic parameter M, the porosity parameter $\widetilde{K}$, the fluid particle interaction parameter βv, and the mass concentration of dust particles l, and nanoparticle size d_n on nanofluid velocity profiles $f(\eta), g(\eta)$, and dust velocity profiles $F(\eta), G(\eta)$ are depicted in Figs. 2-7. For calculations, the range of variations of the following variables is considered:

$$\Lambda = (1, 3, \infty), \quad M = (0.5, 1.5, 2.5), \quad \widetilde{K} = (0.5, 1.5, 2.5),$$

$$\beta_v = (0.3, 0.5, 1), \quad l = (2, 3, 4), \quad d_n = (0.2, 1.2, 2.2),$$

$$c = 0.5, \quad \phi_s = 0.05, \quad h = 1.$$

The effects of Λ, M and $\widetilde{K}$ on the fluid and dust phase velocities of nanofluid Al_2O_3-H_2O are shown in Figs. 2-4. These figures depict that as the values of the parameters Λ, M and $\widetilde{K}$ increase, the velocities of the fluid and dust phases decrease. The physical meaning of the tempo deceleration demonstrated in Fig. 2 is to increase the plastic dynamic viscosity as Λ values increase, creating resistance to the flowing fluid.

A similar behaviour of velocity profiles can be seen in Fig. 3. Since the Lorentz force increases with the value of the magnetic parameter M, we observe that there is some resistance to fluid flow, which leads to a decrease in the flow velocity profiles.

In Fig. 4, the velocities decrease in both directions as the value of the porosity parameter $\widetilde{K}$ in the boundary layer increases. Therefore, the thickness of the boundary layer also decreases at higher values of $\widetilde{K}$.

Fig. 5 shows the influence of the fluid interaction parameter β_v on the velocity of the fluid and dust phases for nanofluid Al_2O_3-H_2O as a function of η. These graphs (Figs. 5a, 5b, and 5c) demonstrate that as β_v increases, the velocities of the fluid phase $f'(\eta), g'(\eta)$ decrease in both lateral directions x and y, while the velocities of the dust phase $F'(\eta), G'(\eta)$ increase. The reason for this is that a larger fluid interaction parameter β_v produces more resistance for the fluid flow phase and less for the dust phase.

Fig. 6 depicts the effect of l on the fluid phase and dust phase velocities of the nanofluid (Al_2O_3-H_2O). This demonstrates that a decrease in the velocity profiles for both the fluid and dust phases is caused by an increase in the parameter l. This is because an increase in the parameter l directly correlates with an increase in dust particle density. The result is an increase in the flow resistance for both the fluid and dust phases.

Fig. 7 illustrates the impact of an increase in nanoparticle diameter d_n on the velocity profiles for the fluid and dust phases. As a result, we can see that as the nanoparticle diameter d_n rises, the fluid and dust phase flows to speed up in the lateral directions x and y, which causes the boundary layer thickness to rise as well. Thus, using the obtained analytical results, one can quickly and easily give a physical interpretation of the processes caused by variations in various flow parameters of a nanofluid containing dust particles without using any numerical methods for solving equations (14)-(17).

Let us compare the known numerical results of Ahmad and Nazar [8], Nadeem et al. [12], Oyelakin et al.[25] and Vajravelu et al. [26] with the results obtained from expressions (21) taking into account (26) and (29) for local skin friction coefficients $-f''(0), -g''(0)$ under the following conditions:

$$\widetilde{K} = 0, \quad \phi_s = 0, \quad \beta_v = 0.$$

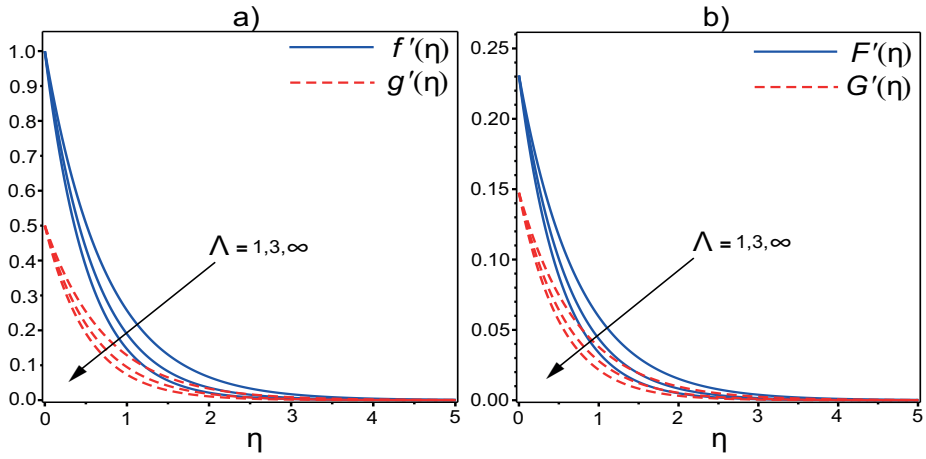

Fig. 2. Influence of Λ on velocity profiles $f'(\eta), g'(\eta)$ and $F'(\eta), G'(\eta)$ at fixed parameters $M = \widetilde{K} = c = 0.5, l = 2, d_n = 0.2, h = 1$ and $\beta_v = 0.3$.

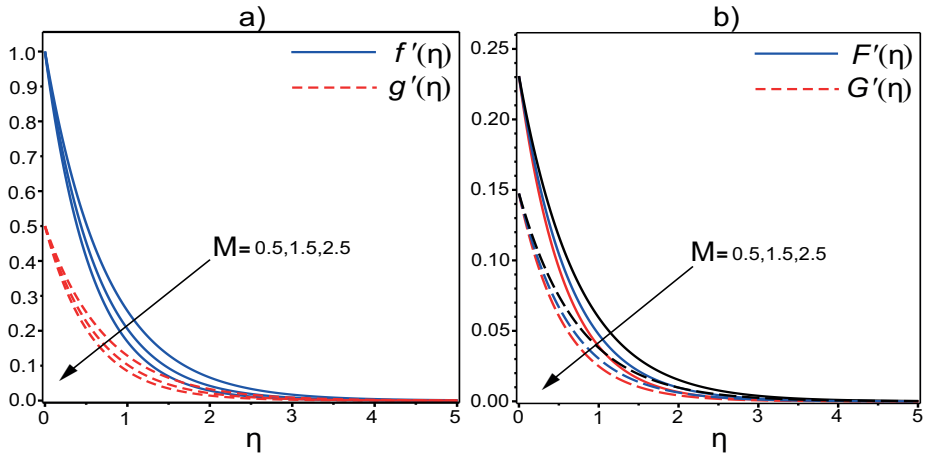

Fig. 3. Effect of M on velocity profiles $f'(\eta), g'(\eta)$ and $F'(\eta), G'(\eta)$ at fixed parameters $\Lambda = 1, \widetilde{K} = c = 0.5, l = 2, d_n = 0.2, h = 1$ and $\beta_v = 0.3$.

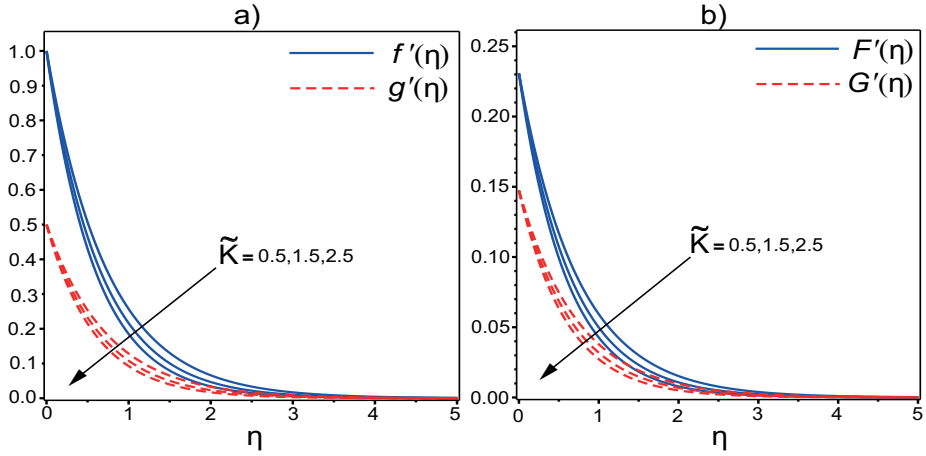

Fig. 4. Effect of $\widetilde{K}$ on velocity profiles $f'(\eta), g'(\eta)$ and $F'(\eta), G'(\eta)$ at fixed parameters $\Lambda = 1, M = c = 0.5, l = 2, d_n = 0.2, h = 1$ and $\beta_v = 0.3$.

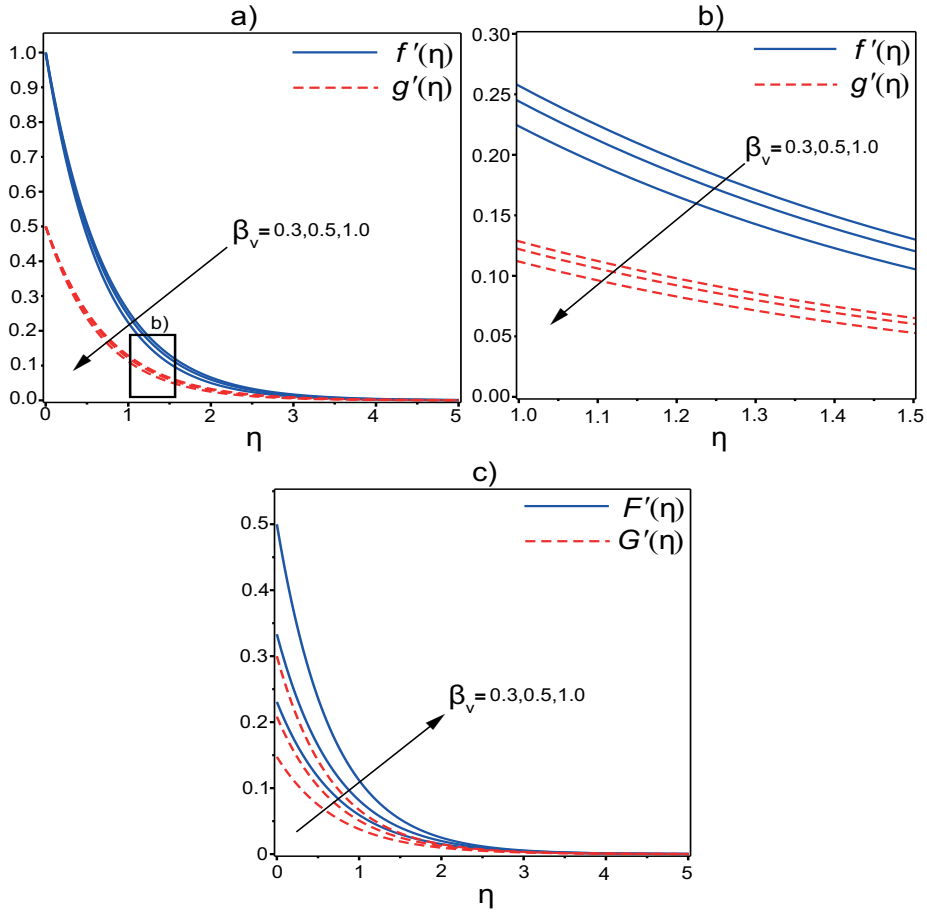

Fig. 5. Influence of β_v on velocity profiles $f'(\eta), g'(\eta)$ and $F'(\eta), G'(\eta)$ at fixed parameters $\Lambda = 1, M = \widetilde{K} = c = 0.5, l = 2, d_n = 0.2, h = 1$.

The analytical results obtained from the exact solutions (29) and the available numerical results [8],[12],[25],[26] agree well, as shown in Tab. 3.

In the case of the flow of a Newtonian electrically conductive fluid with dust particles under the conditions,

$$c = 0, \quad \widetilde{K} = 0, \quad \phi_s = 0,$$

we obtain an exact analytical expression for the coefficient of skin friction, which coincides with the result of Jalil et al.[22]:

$$-f''(0) = \sqrt{1 + M + \frac{\beta_v l}{1 + \beta_v}} \tag{30}$$

The analytical results obtained as a result of the use of expression (30) are perfectly consistent with the numerical results of Gireesha et al. [27].

In the case of the flow of a non-Newtonian electrically conductive nanofluid with dust particles under the conditions,

$$c = 0, \quad \widetilde{K} = 0,$$

we obtain an exact analytical expression for the coefficient of skin friction, which coincides with the result of Khan et al.[27]:

$$-f''(0) = \sqrt{\frac{1}{\left(1 + \frac{1}{\Lambda}\right)\frac{\mu_{nf}}{\mu_f}} \left(\frac{\rho_{nf}}{\rho_f} + \frac{\sigma_{nf}}{\sigma_f} M + \frac{\beta_v l}{1 + \beta_v} \right)} \tag{31}$$

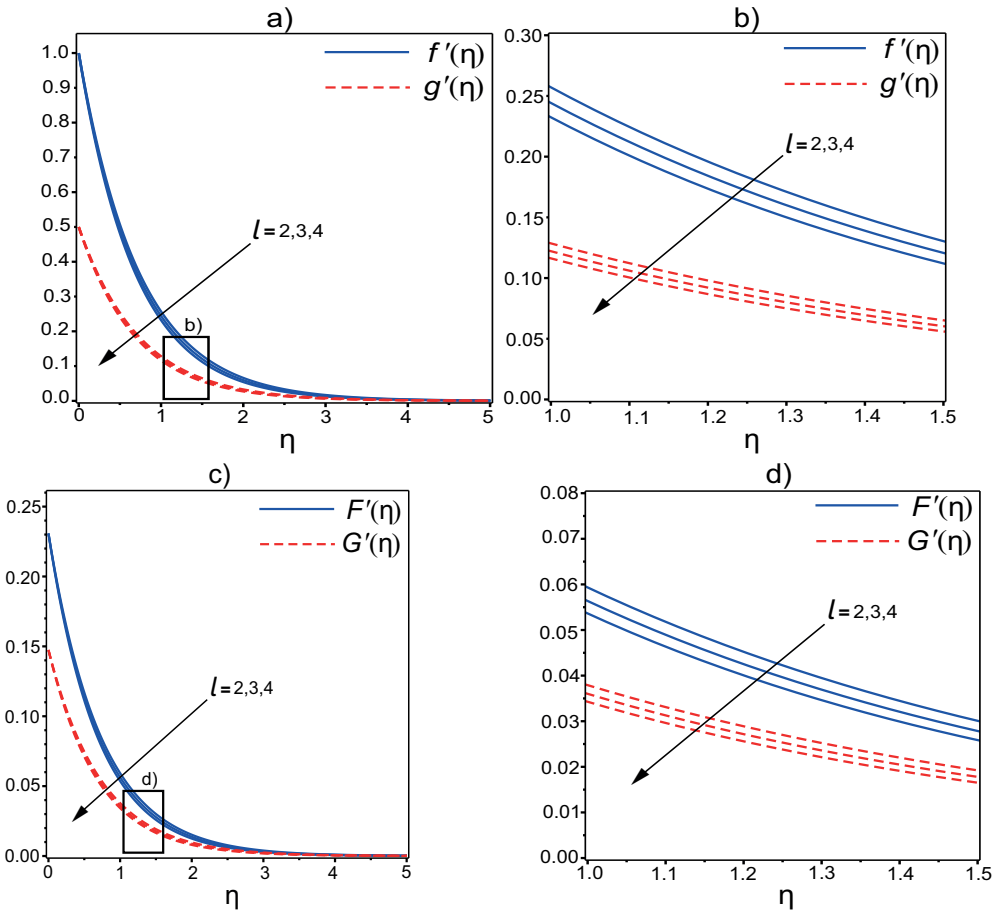

Fig.6. Effect of l on velocity profiles $f'(\eta), g'(\eta)$ and $F'(\eta), G'(\eta)$ at fixed parameters $\Lambda = 1, M = \widetilde{K} = c = 0.5, d_n = 0.2, h = 1$ and $\beta_v = 0.3$.

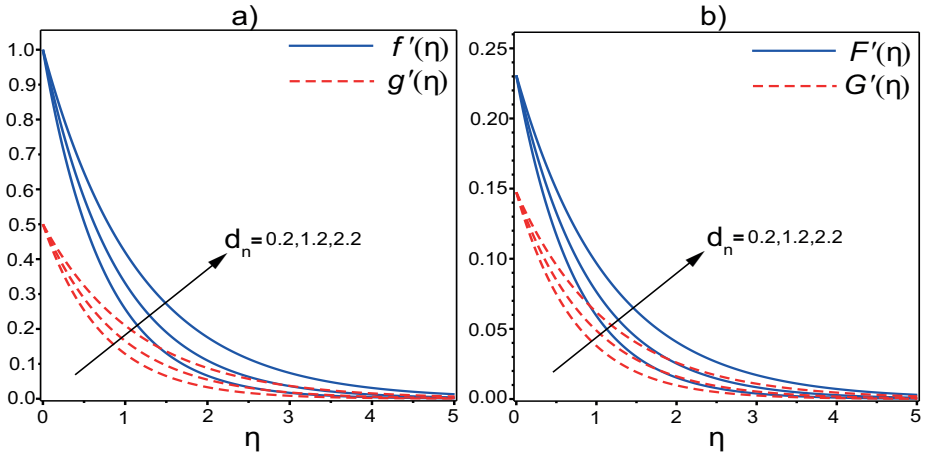

Fig. 7. Effect of d_n on velocity profiles $f'(\eta), g'(\eta)$ and $F'(\eta), G'(\eta)$ at fixed parameters $\Lambda = 1, M = \widetilde{K} = c = 0.5, l = 2, h = 1$ and $\beta_v = 0.3$.

As shown in [22], the analytical results obtained by using the expression (31) are in complete agreement with the numerical results of Vajravelu et al. [26].

Next, we study the influence of the non-Newtonian (Cassonian) parameter Λ, magnetic field M, porosity $\widetilde{K}$, fluid particle interaction parameter β_v, mass concentration of dust particles l, and nanoparticle

Table 2. A comparison of exact solutions for skin friction coefficients $-f''(0)$ and $-g''(0)$ with numerical results [8],[12],[25],[26].

Λ	M	c	$-f''(0)$ numerical results	$-g''(0)$ numerical results	$-f''(0)$ exact solutions	$-g''(0)$ exact solutions
∞	0	0	1.0000 [26] 1.0042 [8],[12]	0	1.0000	0
1	0	0	0.7071 [26]	0	0.7071	0
2	0	0	0.8164 [26]	0	0.8164	0
3	0	0	0.8660 [26]	0	0.8660	0
4	0	0	0.8944 [26]	0	0.8944	0
∞	0	0.5	1.0932 [8],[12]	0.4653 [8],[12]	1.2247	0.6123
∞	10	0.5	3.3420 [8],[12]	1.6459 [8],[12]	3.3911	1.6955
∞	100	0.5	10.058 [8],[12]	5.0208 [8],[12]	10.074	5.0373
1	10	0	2.3452 [25]	0	2.3452	0
1	10	0.5	2.3631 [25]	1.1638 [25]	2.3979	1.1989
5	10	0	3.0276 [25]	0	3.0276	0
5	10	0.5	3.0508 [25]	1.5025 [25]	3.0956	1.5478

Table 3. Values $-f''(0)$ and $g''(0)$ for the steady flow of a dusty nanofluid with various variations of parameters.

Λ	M	$\widetilde{K}$	β_v	l	d_n	$-f''(0)$	$-g''(0)$
1	0.5	0.5	0.3	2	0.2	1.3582	0.6791
3	0.5	0.5	0.3	2	0.2	1.6635	0.8317
∞	0.5	0.5	0.3	2	0.2	1.9209	0.9604
1	1.5	0.5	0.3	2	0.2	1.5823	0.7911
1	2.5	0.5	0.3	2	0.2	1.7784	0.8892
1	0.5	1.5	0.3	2	0.2	1.5313	0.7656
1	0.5	2.5	0.3	2	0.2	1.6867	0.8433
1	0.5	0.5	0.5	2	0.2	1.4097	0.7048
1	0.5	0.5	1.0	2	0.2	1.4977	0.7488
1	0.5	0.5	0.3	3	0.2	1.4096	0.7048
1	0.5	0.5	0.3	4	0.2	1.4592	0.7296
1	0.5	0.5	0.3	2	1.2	1.1053	0.5526
1	0.5	0.5	0.3	2	2.2	0.8682	0.4341

size d_n on local skin friction coefficients $-f''(0), -g''(0)$ for nanofluid Al_2O_3-H_2O. The physical properties of the nanofluid are taken from Tab. 2. We select the following fixed parameters for the problem: $c = 0.5, \phi_s = 0.05, h = 1$. The numerical values $-f''(0), -g''(0)$ for various variations of $\Lambda, M, \widetilde{K}, \beta_v, l$, and d_n are then obtained using the exact solutions (26) and (29), as shown in Tab. 4. Tab. 4 shows that, at the limit of the Newtonian fluid ($\Lambda = \infty$) the surface friction coefficients of the nanofluid in the x and y directions are higher than those of the non-Newtonian fluid. In addition, an increase in the parameters $\Lambda, M, \widetilde{K}, \beta_v$, and l reduces the fluid flow velocity, which leads to an increase in the absolute values of the skin friction coefficients in the x and y directions. On the other hand, as the nanoparticle diameter d_n

increases, so does the fluid flow velocity, which naturally leads to a decrease in the coefficients of surface friction in the x and y directions.

5. Conclusions

In the present study, for the first time, an analytical solution for a stationary MHD boundary flow of a Cassonian nanofluid containing dust particles over a stretching sheet is obtained. In the lateral directions x and y, a variant of linear stretching of a sheet (see Fig. 1) is considered. Analytical expressions for the velocities of the fluid and dust phases, as well as skin friction in lateral directions x and y, are derived for the flow of a typical nanofluid (Al_2O_3-H_2O).The influence of the Casson parameter Λ, the magnetic parameter M, the porosity parameter $\widetilde{K}$, the fluid-particle interaction parameter β_v, the mass concentration of dust particles l, and the nanoparticle size d_n on the velocity profiles of the fluid and dust phases is studied. New results for skin friction coefficients in lateral directions are presented in Table 3. For simpler physical situations, comparison of the analytical results with the numerical results of previous studies showed a high level of accuracy and consistency. The main results of this study are as follows:

1. An increase in the parameters $\Lambda, M, \widetilde{K}$, and l leads to a decrease in the flow rate of the fluid and dust phases.

2. It is found that the velocity of the fluid phase decreases due to an increase in the parameter β_v, while the velocity of the dust phase increases.

3. An increase in the diameter d_n of aluminium oxide nanoparticles leads to a decrease in the viscosity of the water-based nanofluid and, as a consequence, an increase in the flow rates of the fluid and dust phases.

Building upon our work, future analytical solutions will describe the unsteady 3D MHD Casson flow of non-Newtonian dusty fluids over a porous stretching surface.

References

1. P. G. Saffman, *J. Fluid Mech.*, **13**, 120 (1962).
2. K. M. Chakrabarti, *AIAA Journal*, **12**(8), 1136 (1974).
3. N. Datta and S. K. Mishra, *Acta Mech.*, **42**, 71 (1982).
4. B. C. Sakiadis, *AIChE J.*, **7**, 221 (1961).
5. F. K. Tsou, E. M. Sparrow, R. J. Goldstein, *International Journal of Heat and Mass Transfer*, **10**, 219 (1967).
6. L. Crane, *Z. Angew. Math. Phys.*, **21**, 645 (1970).
7. C. Y. Wang, *Phys. Fluids* **27**, 1915 (1984).
8. K. Ahmad, R. Nazar, *J. Sci. Technol.*, **3**(1), 33 (2011).
9. S. U. S. Choi, J. A. Eastman, *Am. Soc. Mech. Eng. Fluids Eng. Div. FED*, **231**, 99 (1995).
10. M. Ramzan, S. Inam, S. A. Shehzad, *Alex. Eng. J.*, **55**, 311 (2015).
11. M. B. Ashraf, T. Hayat, M. S. Alhuthali, *J. Aerosp. Eng.*, **29**, 04015065-1-8 (2016).
12. S. Nadeem, R. U. Haq, N. S. Akbar, Z. H. Khan, *Alex. Eng. J.*, **52**, 577 (2013).
13. S. Nadeem, R. U. Haq, N. S. Akbar, *IEEE TNANO*, **13**, 108 (2014).
14. G. Mahanta, S. Shaw, *Alex. Eng. J.*, **54**, 653 (2015).
15. M. Krishna Murthy, *Int. J. Chem. Eng. Res.*, **41**, 29 (2016).
16. S. Madhusudan, S. Kharabela, and P. S. Kumar, *Karbala Int. J. Mod. Sci.*, **6**(1), 93 (2020).
17. W. Ibrahim and T. Anbessa, *Hindawi Math. Probl. Eng.*, **2020**, Article ID 8656147, 15 (2020).
18. M. Jalil, S. Asghar, Sh. Yasmeen, *Hindawi Math. Probl. Eng.*, **2017**, Article ID 2307469, 5 (2017).
19. A. B. Vishalakshi, U. S. Mahabaleshwar, and I. E. Sarris, *Micromachines*, **13**, 116 (2022).
20. U. S. Mahabaleshwar, T. Anusha, D. Laroze, N. M. Said and M. Sharifpur, *Sustainability*, **14**, 7020 (2022).
21. A. B. Vishalakshi, U. S. Mahabaleshwar, and M. Hatami, *Sci. Rep.* **12**, 16071 (2022).
22. U. Khan, F. M. Oudina, A. Zaib, A. Ishak, S. A. Bakar, El-Sayed M. Sherif, and D. Baleanu, *Waves Random Complex Media*, (2022) Published online: 25 Jul 2022.

23. M. I. Kopp, U. S. Mahabaleshwar, L. M. Pérez, *J. Phys. Stud.*, **27**(2), 2402 (2023).
24. A. A. Akbar, N. A. Ahammad, A. U. Awan, A. K. Hussein, F. Gamaoun, E. M. Tag-ElDin, B. Ali, *Nanomaterials*, **12**, 2801 (2022).
25. I. S. Oyelakin, S. Mondal, P. Sibanda, *Front. Heat Mass Transf.*, **8**, 37 (2017).
26. K. Vajravelu, K. V. Prasad, H. Vaidya, N. Z. Basha, Chiu-On Ng, *Int. J. Appl. Comput. Math.*, **3**, 1619 (2017).
27. B. J. Gireesha, G. K. Ramesh, and C. S. Bagewadi, *Adv. Appl. Sci. Res.*, **3**, 2392 (2012).